MERIT Self-directed joint research report

# Elucidation of low-temperature phases in a two-dimensional material MXene

Yuji Nakagawa and Yusuke Morikawa

**Abstract –** Since the appearance of graphene, various two-dimensional materials have been attracting growing interest. Among them, MXene has a unique structure in which each layer is functionalized. Despite the prediction of superconductivity and magnetism depending on the composition and functional group, no phase transition has been observed yet. In this study, the resistance of MXene was modulated by intercalation and measured down to low temperature. Although no phase transition appeared, the resistance was substantially reduced with intercalation, indicating the intercalation is an effective method to realize ordered phases in MXene.

## 1. Authors information

**Yuji Nakagawa –** He belongs to Iwasa/Nakano laboratory in the department of applied physics. His specialties are electrochemical control and resistance measurement of layered materials.

**Yusuke Morikawa –** He belongs to Yamada/Okubo laboratory in the department of chemical system engineering. His specialties are synthesis and analysis of electrodes for secondary batteries.

## 2. Introduction and purposes of this work

Motivated by the great success of graphene [1], two-dimensional (2D) materials having layered crystal structures have been widely studied. A variety of 2D materials including transition metal dichalcogenides, such as $MoS_2$ [2,3,4], $NbSe_2$ [5] and $WTe_2$ [6], hexagonal boron nitride hBN [7], black phosphorus S [8], transition metal chloronitrides ZrNCl and HfNCl [9], iron selenide FeSe [10], and one of the cuprates $Bi_2Sr_2CaCu_2O_{8+x}$ [11] are studied from multiple aspects like low temperature physics such as superconductivity [3-5, 9-11] or device application such as transistor operation [2,8]. Most recently, 2D magnets $Cr_2Ge_2Te_6$ [12] and $CrI_3$ [13] are attracting renewed interest, which shows that development of new materials and new properties is the driving force for promoting researches in 2D materials.

MXene, the object of this research, is a 2D material synthesized in 2011 [14]. It is a layered transition metal carbide (or nitride, carbonitride) and is expressed by the composition formula $M_{n+1}X_nT_x$, where $M$, $X$, and $T$ denote transition metals, C or N, and functional group, respectively. MXene is obtained from MAX phases $M_{n+1}AX_n$ by selective etching of $A$ atoms such as Al, Si, P, and S (Fig. 1a). Because more than 60 kinds of MAX phases have been reported, a large variety of MXene is thought to be exist, and indeed, MXenes with $n$ = 1, 2, 3; $M$ = Sc, Ti, V, Cr, Zr, Nb, Mo, Hf, Ta; $X$ = C, N are successfully synthesized [15]. The most unique feature of MXene, the functional group $T$ = O, OH, Cl, F, ... attaching to both sides of each layer, further increases the degree of freedom of material design in MXene. It is theoretically predicted that MXene becomes a superconductor, topological insulator, magnetic material depending on composition and functional group [15]. However, there are still few experimental reports of MXene, and no observation of these physical properties has been done.

As well as other 2D materials, MXene has also attracted attention in application field. Due to the interlayer spacing expanded by functional groups, various cations such as $Li^+$, $Na^+$, $K^+$, $NH^{4+}$, $Mg^{2+}$, $Al^{3+}$ are easily intercalated [16]. MXene is known as a candidate material for electrodes not only in Li-ion

batteries, but also in next-generation secondary batteries such as Na-ion batteries [17].

In the viewpoint of physics, intercalation is a doping method commonly used in 2D materials. Transition metal dichalcogenides [18,19], black phosphorus [20], and transition metal chloronitrides [9] are known for their superconducting phases induced by electron doping via intercalation. Since intercalation is also applicable to MXene, it is possible to search for ordered phases in MXene by combining multiple degrees of freedom, that is, composition, functional group, and intercalation. Low temperature measurements of intercalated MXene have been reported in $Ti_3C_2T_x$ with $n$ = 2 [21]. The resistivity is increased after the intercalation of $NH_4^+$ and $NH_3$, indicating that the carrier doping is not effective in this case. Intercalation of metal atoms seems to be needed for exploring ordered phases such as superconductivity. Also, it is important to study $M_2XT_x$ with $n$ = 1, because with smaller $n$, each layer become thinner and more sensitive to the intercalation.

Based on the above background, in this joint research, we tried to clarify the low temperature properties of intercalated MXene and aimed to be a pioneer in the study of physical properties in MXene. We focused on $Ti_2CT_x$, which is the most common composition among MXenes of $n$ =1. Functional groups were not evaluated in this study, but in a previous study $T$ is clarified as $(OH)_{0.3}O_{0.7}F_{0.6}Cl_{0.4}$ under the same synthesis condition as in our study [22]. Lithium was used as intercalant.

Yuji Nakagawa has a technique to intercalate ions into 2D materials and measure its resistance at low temperature. Yusuke Morikawa has abundant experiences of synthesizing materials for electrodes used in secondary batteries, and it is possible to synthesize MXene. Therefore, we thought that we could achieve the above purpose through this self-directed joint research.

## 3. Methods

In this research, Morikawa is in charge of the synthesis of MXene, while Nakagawa was responsible for intercalation and resistance measurement.

### 3.1 Synthesis of MXene

MXene is synthesized by selective etching of $A$ layer from the mother layered compound, MAX phases [14,22].

MAX phase $Ti_2AlC$ was synthesized by solid phase method. TiC (> 99%, Kojundo Chemical), Ti (> 99%, Kojundo Chemical) and Al (> 99.9%, Kojund Chemical) were mixed using a planetary ball mill and heated at 1673 K under Ar atmosphere for 1 hour. The obtained $Ti_2AlC$ was pulverized again by a planetary ball mill. We added it to 6 M HCl aqueous solution in which LiF was dissolved at a concentration of 0.9 M and stirred at 313 K for 20 hours for the selective etching of Al. After that, the powder was dried at 473 K in vacuum for 20 hours to remove $H_2O$ between layers. The crystal structure of the powder is determined to be $Ti_2CT_x$ by XRD analysis.

### 3.2 Preparation for measurement

The grain size of MXene powder obtained above is in the scale of μm. To isolate and measure single crystal, the powder was adhered to Scotch tape, and the tape was attached to the $Si/SiO_2$ substrate. After peeling off the tape, most of the crystals remain on the tape, but some crystals are transferred to the substrate, resulting in isolated MXene. This is the same process used to obtain graphene [1].

Subsequently, electrodes were fabricated by electron beam lithography in Hall-bar geometry. The gate electrode used for intercalation (explained later) is also deposited at the same time. After the fabrication of electrodes, a resist for electron beam lithography is spin-coated again, and the edges of the sample and the gate electrode are developed (Fig. 2a). Therefore, sample channel and other electrodes are protected by resist.

After bonding the gold wires, we put Li electrolyte and set it in Physical Properties Measurement System (PPMS, Quantum Design). As the Li electrolyte, $LiClO_4$ dissolved in PEO (molecular weight: 600) was used. The thickness of the sample was measured using an atomic force microscope (AFM).

### 3.3 Intercalation

Intercalation is carried out using the ionic-gating method [18, 19]. The gate electrode and sample are covered with the Li electrolyte. When we applied positive gate voltage $V_G$ to the gate electrode, Li ions are accumulated on the sample and eventually intercalated into the sample. Since the resistance of the sample decreases by doping via intercalation, it can be regarded as a transistor operation, whereas it is the same reaction as in the Li-ion battery. This operation was carried out at room temperature 300 K under high vacuum.

### 3.4 Resistivity measurement

Resistivity was measured in 4-terminal AC setup with low frequency. Not only the temperature and magnetic field dependence, but also $V_G$ dependence is measured. We note the source drain voltage $V_{DS}$ is about 1 mV, which is negligibly small comparing to $V_G$ of several volt.

## 4. Results and discussion

### 4. 1 Characterization of MXene

Figure 1a and 1b show the crystal structure and the XRD pattern of $Ti_2AlC$ (MAX phase) and $Ti_2CT_x$ (MXene), respectively. After the LiF/HCl etching, (002) peak near 10° was shifted to the lower angle, indicating the expansion of the interlayer spacing due to the functional group and thus the successful conversion to MXene. The broadened peak corresponds to the laminated structure due to the etching process. Using the angle of (002) peak, the interlayer distances of $Ti_2AlC$ and $Ti_2CT_x$ were calculated to be 6.8 Å and 9.2 Å, respectively. The latter value is larger than the value of 8.7 Å in the previous study [22]. Therefore, the proportion of Cl in the functional group $T$ seems to be larger in our samples. Although some amount of $Ti_2AlC$ remains unconverted in $Ti_2CT_x$ powder, it can be excluded in our single particle measurement.

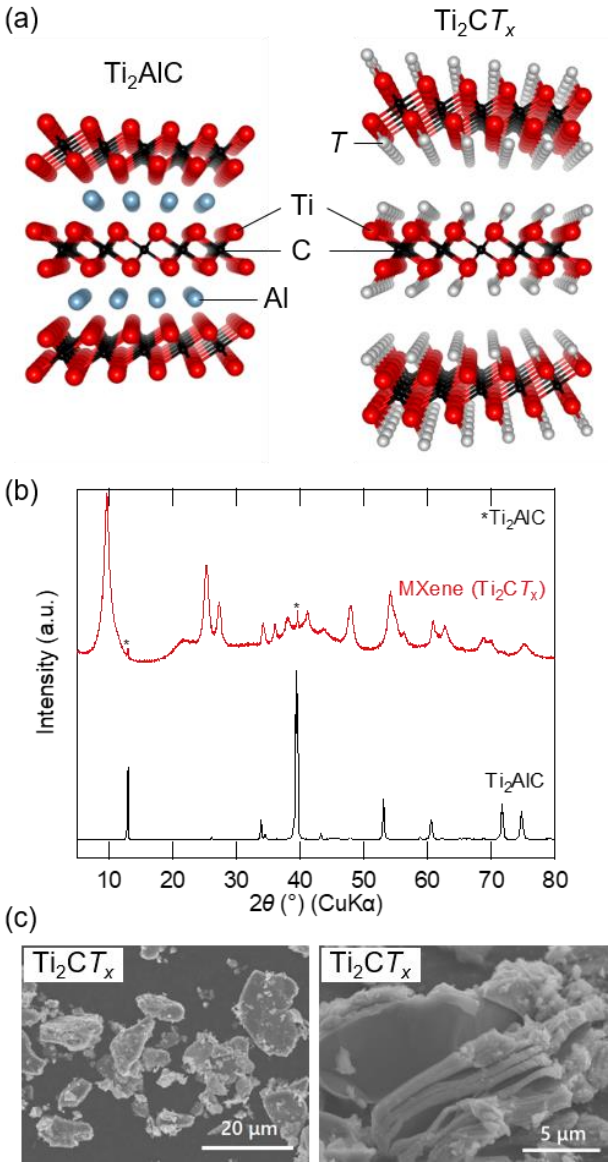


**Figure 1: (a) Crystal structure and (b) XRD pattern of precursor $Ti_2AlC$ and MXene $Ti_2CT_x$.** In $Ti_2CT_x$, functional group $T$ enlarges the interlayer spacing. **(c) SEM image of $Ti_2CT_x$.** Stacking structures are visible.

Scanning electron microscopy (SEM) image of $Ti_2CT_x$ is shown in Fig. 1c. The particle size of $Ti_2CT_x$ was about 5-20 μm. The stacked structure reflecting the layered structure and its delamination was clearly observed.

One piece of MXene was isolated from the powder and electrodes were fabricated in the above process (Fig. 2a). The resistivity at room temperature was 3-50 mΩ cm depending on samples. In the previous studies, the resistivity of $Ti_2CT_x$ was reported as 280 Ω/sq [23]. Assuming the thickness to be 100 nm, that value corresponds to 2.8 mΩ cm, which is smaller than ours. Also, resistivity of $Ti_3C_2T_x$ was reported to be 0.2 - 40 mΩ cm [21].

The difference should originate from different synthesis methods, which leads to the different ratio of functional groups and to the different interlayer distance [22]. The sample used in this study contains Cl as a functional group, and the interlayer distance is elongated. On the other hand, the thickness of each layer is related to $n$, which is 1 for $Ti_2CT_x$ and 2 for $Ti_3C_2T_x$. Therefore, our sample has the smallest conducting part per unit volume, and it is reasonable that our sample has relatively high resistivity.

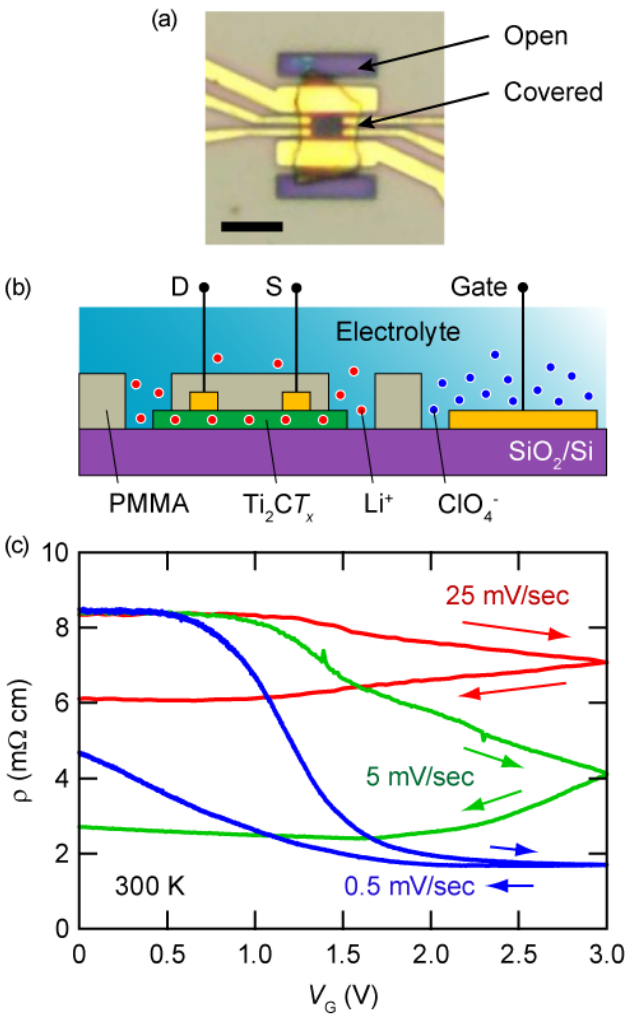


**Figure 2: Device structure and intercalation operation** (a) optical microscope image of the device. Electrodes are fabricated in Hall-bar geometry, and the device is covered with PMMA resist except for the edges of the sample. Scale bar, 5 μm. (b) Illustration of the device operation (side view). After dropping electrolytes, gate voltage $V_G$ is applied. At the same time, resistance was measured with small Source-Drain voltage. (c) $V_G$ dependence of resistivity. It depends on the sweeping speed.

### 4. 2 Intercalation operation

After dropping the lithium electrolyte, we applied $V_G$ in the positive direction to intercalate Li ions. The resistance was decreased due to the electron doping (Fig. 2c.

Figure 2c shows a typical intercalation operation. $V_G$ was swept at different speeds with an interval of 10 hours or more between each sweep. In this sample, the initial resistivity was 8.4 mΩ cm, but the resistance decreased to 1.7 mΩ cm by the intercalation.

The sweep was performed at 0.5, 5, and 25 mV/sec, which took 200, 20, and 4 minutes for the sweep. In all cases, the resistance decreases with applying $V_G$. However, the threshold voltage at which the resistance starts to decrease depends on the sweep speed. The faster sweep shifts the threshold to the higher voltage

side. In the case of the slowest sweeping speed 0.5 mV/sec, the drop was saturated at $V_G$ = 3 V. At faster sweeping rates of 5, 25 mV/sec, the resistance kept decreasing even in the reverse sweep. The difference depending on the sweep rate reflects charging speed of intercalation in $Ti_2CT_x$. The cyclic voltammetry (CV) measurement in a lithium ion battery configuration also indicates that the intercalation takes a certain amount of time[22].

Even with the sufficiently slow sweep rate of 0.5 mV/sec, the sweeping in the negative direction exhibited large hysteresis. It seems long as the time taken for the intercalation process in a microscale single crystal, but large hysteresis is also observed at the sweep rate of 1 mV/sec in $TaS_2$ using similar method [18]. The difference between $V_G$ and actual applied voltage to the sample, which should be measured in further studies, could be one of the origin of the hysteresis.

We confirmed the large resistance drop by intercalation in many samples. We tried applying larger $V_G$, such as 15 V, but further resistance drop was not observed.

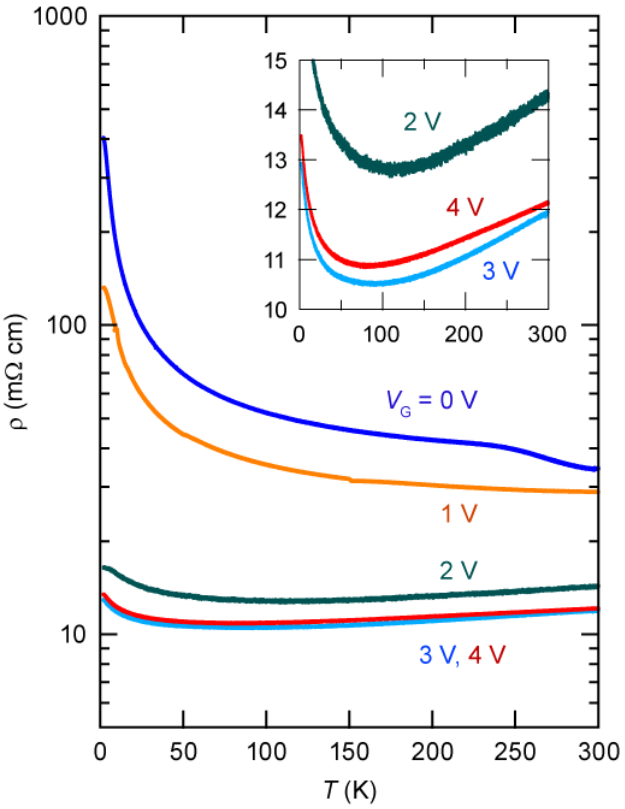


**Figure 3: Temperature dependence of $Li_yTi_2CT_x$** Resistivity decreases with applying $V_G$, which results in the metallic behavior. Inset: linear plot of the small resistivity region.

### 4. 3 Temperature dependence of resistivity

Intercalation by the ionic gating method was found to be effective in $Ti_2CT_x$. Subsequently, we measured the temperature dependence of the resistivity at each gate voltage. Before cooling, we applied certain $V_G$ at 300 K and waited for for 1 hour or more until the resistance became stable.

The results are shown in Fig. 3. The cooling scans were performed in the order of $V_G$ = 0, 3, 2, 4, 1 V. Although the resistivity is low even before applying voltage ($V_G$ = 0 V), it shows insulating behavior. By applying $V_G$ larger than 2 V, metallic behavior appeared with which resistance decreases to 100 K on cooling. Although resistance increases at low temperature, it is not a sharp rise as before applying $V_G$.

The resistances at $V_G$ = 3, 4 V are almost identical, which agrees with the result of $V_G$ sweep (Fig. 2). The slightly higher resistance at $V_G$ = 4 V should be attributed to the damage caused by repeated cooling.

No indication of superconductivity was observed, but in the case of $V_G$ = 0 V, the bending of the resistance curve was observed at a relatively high temperature of about 250 K. This bending, which disappears when $V_G$ is applied, might suggest some phase transition, though it is not clarified in our study.

### 4. 4 Hall measurement

The intercalated Li atoms supply electrons to $Ti_2C$ layer. Assuming perfect carrier transfer that the number of Li atoms equals to the number of electrons, the

doping level can be calculated from Hall coefficient. Magnetic field was swept at 150 K, at which the intercalation reaction doesn't occur.

Figure 4(a) and (b) show the result at $V_G$ = 0 V and 1-4 V, respectively. The transverse resistance was antisymmetrized to the magnetic field. Although at $V_G$ = 0 V the data have many noises, reproducible Hall resistance independent of the sweep direction was obtained. By applying $V_G$, the signal became clearer and the slope became smaller. These lines were fitted with a linear function to derive Hall coefficients.

The inverse of the Hall coefficients increased by applying $V_G$ and saturates at 3 V, showing similar consistent behavior with resistivity. This should reflect the increased carrier density due to intercalation.

In the Drude model describing electric conduction, the value of $1/eR_H$ corresponds to the carrier density. By calculating this value, we got $1/eR_H = 4.7 \times 10^{21}$ /cm$^3$ before voltage application, corresponding to the situation where 0.36 electrons exist per Ti atom. On the other hand, ten times larger value of $4.5 \times 10^{22}$ / cm$^3$ was obtained at $V_G$ = 3 V. This corresponds to the situation where 3.4 electrons exist per Ti atom and approximately 3 electrons are supplied to each Ti atom by Li intercalation. This doesn't correspond to the actual situation, and we can say that the Drude model cannot be applied to $Ti_2CT_x$. It could be because of the complex band structure of $Ti_2CT_x$.

Although it is difficult to derive the number of carriers or the doping level, the Hall coefficients systematically changed on applying $V_G$, which possibly reflects the change of the electronic state.

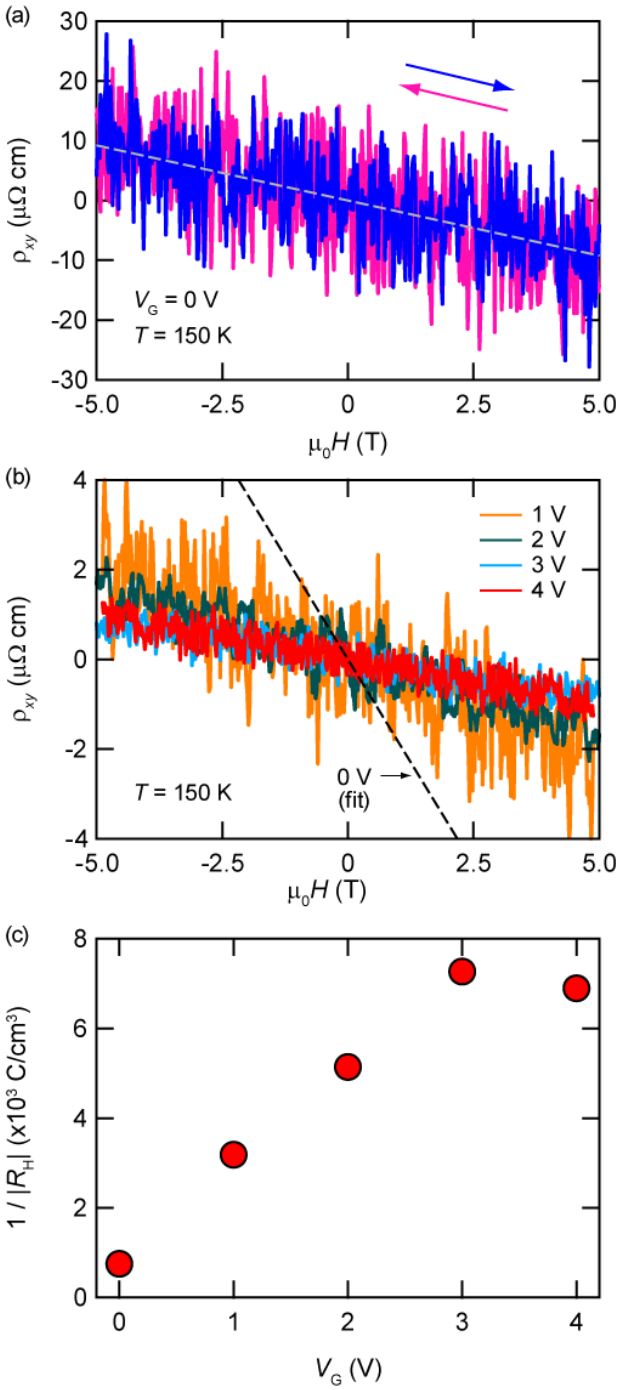


**Figure 4: Hall measurement in $Li_yTi_2CT_x$** Measurement results at (a) $V_G$ = 0 V, (b) $V_G$ = 1-4 V at 150 K. **(c)** $V_G$ dependence of the inverse of Hall coefficient.

## 5. Summary and outlook

In this study, Li intercalation was performed on MXene $Ti_2CT_x$, and resistivity and Hall coefficient were investigated *in-situ*. Resistance was decreased, and its temperature dependence changed from insulating to metallic by the electron doping. It indicates that the intercalation is effective to pursue the expected physical properties in MXene.

The bending of the resistance seen at 250 K, the net potential change during $V_G$ sweep, and the band structure of $Ti_2CT_x$ are remained to be investigated. Furthermore, we are now trying to measure other MXene, like $Nb_2CT_x$, to observe the superconducting transition, which is absent in our present study.


## 6. Acknowledgement

We would like to thank the supports and encouragement of our supervisors, professor Yoshihiro Iwasa, professor Atsuo Yamada, and professor Masashi Kawasaki. We also thank the MERIT program for providing us the valuable chance of doing this interdisciplinary research.


## 7. References


1. K. S. Novoselov, A. K. Geim, S. V. Morozov, D. Jiang, Y. Zhang, S.V. Dubonos, I. V. Grigorieva & A. A. Firsov, Electric field effect in atomically thin carbon films. *Science* **306**, 666 (2004).
2. B. Radisavljevic, A. Radenovic, J. Brivio, I. V. Giacometti & A. Kis, Single-layer $MoS_2$ transistors. *Nature Nanotechnology* **6**, 147 (2011).
3. J. T. Ye, Y. J. Zhang, R. Akashi, M. S. Bahramy, R. Arita & Y. Iwasa, Superconducting dome in a gate-tuned band insulator. *Science* **338**, 1193 (2012).
4. Y. Saito, Y. Nakamura, M. S. Bahramy, Y. Kohama, J. T. Ye, Y. Kasahara, Y. Nakagawa, M. Onga, M. Tokunaga, T. Nojima, Y. Yanase & Y. Iwasa, Superconductivity protected by spin-valley locking in ion-gated $MoS_2$. *Nature Physics* **12**, 144 (2015).
5. X. Xi, Z. Wang, W. Zhao, J. H. Park, K. T. Law, H. Berger, L. Forro, J. Shan & K. F. Mak, Evidence of Ising pairing in superconducting $NbSe_2$ atomic layers. *Nature Physics* **12**, 139 (2015).
6. A. A. Soluyanov, D. Gresch, Z. Wang, Q. Wu, M. Troyer, X. Dai & B. A. Bernevig, Type-II Weyl semimetals. *Nature* **527**, 495 (2015).
7. K. Watanabe, T. Taniguchi & H. Kanda, Direct-bandgap properties and evidence for ultraviolet lasing of hexagonal boron nitride single crystal. *Nature Materials* **3**, 404 (2004).
8. L. Li, Y. Yu, G. J. Ye, Q. Ge, X. Ou, H. Wu, D. Feng, X. H. Chen & Y. Zhang, Black phosphorus field-effect transistors. *Nature Nanotechnology* **9**, 372 (2014).
9. Y. Kasahara, K. Kuroki, S. Yamanaka & Y. Taguchi, Unconventional superconductivity in electron-doped layered metal nitride halides *MNX* (*M*= Ti, Zr, Hf; *X*= Cl, Br, I). *Physica C* **514**, 354 (2015).
10. J. F. Ge, Z. L. Liu, C. Liu, C. L. Gao, D. Qian, Q. K. Xue & J. F. Jia, Superconductivity above 100 K in single-layer FeSe films on doped $SrTiO_3$. *Nature Materials* **14**, 285 (2015).
11. D. Jiang, T. Hu, L. You, Q. Li, A. Li, H. Wang, G. Mu, Z. Chen, H. Zhang, G. Yu, J. Zhu, Q. Sun, C. Lin, H. Xiao, X. Xie & M. Jiang, High-$T_c$ superconductivity in ultrathin $Bi_2Sr_2CaCu_2O_{8+x}$ down to half-unit-cell thickness by protection with graphene. *Nature Communications* **5**, 5708 (2014).

12. C. Gong, L. Li, Z. Li, H. Ji, A. Stern, Y. Xia, T. Cao, W. Bao, C. Wang, Y. Wang, Z. Q. Qiu, R. J. Cava, S. G. Louie, J. Xia. & X. Zhang, Discovery of intrinsic ferromagnetism in two-dimensional van der Waals crystals. *Nature* **546**, 265 (2017).
13. B. Huang, G. Clark, E. Navarro-Moratalla, D. R. Klein, R. Cheng, K. L. Seyler, D. Zhong, E. Schmidgall, M. A. McGuire, D. H. Cobden, W. Yao, D Xiao, P. Jarillo-Herrero & X. Xu, Layer-dependent ferromagnetism in a van der Waals crystal down to the monolayer limit. *Nature* **546**, 270 (2017).
14. M. Naguib, M. Kurtoglu, V. Presser, J. Lu, J. Niu, M. Heon, L. Hultman, Y. Gogotshi & M. W. Barsoum, Two-dimensional nanocrystals produced by exfoliation of $Ti_3AlC_2$. *Advanced Materials* **23**, 4248 (2011).
15. M. Khazaei, A. Ranjbar, M. Arai, T. Sasaki & S. Yunoki, Electronic properties and applications of MXenes: a theoretical review. *Journal of Materials Chemistry C* **5**, 2488 (2017).
16. M. R. Lukatskaya, O. Mashtalir, C. E. Ren, Y. Dall'Agnese, P. Rozier, P. L. Taberna, M. Naguib, P. Simon, M. W. Barsoum & Y. Gogotsi, Cation Intercalation and High Volumetric Capacitance of Two-Dimensional Titanium Carbide. *Science* **341**, 1502 (2013).
17. X. Wang, S. Kajiyama, H. Iinuma, E. Hosono, S. Oro, I. Moriguchi, M. Okubo & A. Yamada, Pseudocapacitance of MXene nanosheets for high-power sodium-ion hybrid capacitors. *Nature Communications* **6**, 6544 (2015).
18. Y. Yu, F. Yang, X. F. Lu, Y. J. Yan, Y. H. Cho, L. Ma, X. Niu, S. Kim, Y. W. Son, D. Feng, S. Li, S. W. Cheong, X. H. Chen & Y. Zhang, Gate-tunable phase transitions in thin flakes of 1T-$TaS_2$. *Nature Nanotechnology* **10**, 270 (2015).
19. W. Shi, J. T. Ye, Y. J. Zhang, R. Suzuki, M. Yoshida, J. Miyazaki, N. Ionue, Y. Saito & Y. Iwasa, Superconductivity series in transition metal dichalcogenides by ionic gating. *Scientific Reports* **5**, 12534 (2015).
20. R. Zhang, J. Waters, A. K. Geim & I. V. Grigorieva, Intercalant-independent transition temperature in superconducting black phosphorus. *Nature Communications* **8**, 15036 (2017).
21. J. Halim, M. R. Lukatskaya, K. M. Cook, J. Lu, C. R. Smith, C. R., L. Å. Näslund, S. J. May, L. Hultman, Y. Gogotsi, P. Eklund & M. W. Barsoum, Transparent conductive two-dimensional titanium carbide epitaxial thin films. *Chemistry of Materials* **26**, 2374 (2014).
22. S. Kajiyama, L. Szabova, H. Iinuma, A. Sugahara, K. Gotoh, K. Sodeyama, Y. Tateyama, M. Okubo & A. Yamada, Enhanced Li-Ion Accessibility in MXene Titanium Carbide by Steric Chloride Termination. *Advanced Energy Materials* **7**, 1601873 (2017).
23. S. Lai, J. Jeon, S. K. Jang, J. Xu, Y. J. Choi, J. H. Park, E. Hwang & S. Lee, Surface group modification and carrier transport properties of layered transition metal carbides ($Ti_2CT_x$, T: –OH, –F and –O). *Nanoscale* **7**, 19390 (2015).